

Fluid Mechanics of the eye: linear stability analysis of a two-liquid interface in the vitreous chamber and flow of aqueous humour with an intraocular lens

Jan Pralits

Department of Civil, Chemical and Environmental Engineering
University of Genoa, Italy
jan.pralits@unige.it

December 9, 2014

The work presented has been carried out by:

- **Rodolfo Repetto** DICCA, University of Genoa, Italy;
- **Jennifer Siggers** Imperial College London, UK;
- **Jan Pralits** DICCA, University of Genoa, Italy;
- **Alessandro Stocchino** DICCA, University of Genoa, Italy;
- **Krystyna Isakova** DICCA, University of Genoa, Italy;
- **Julia Meskauskas** DISAT, University of L'Aquila, Italy;
- **Andrea Bonfiglio** DICCA, University of Genoa, Italy.

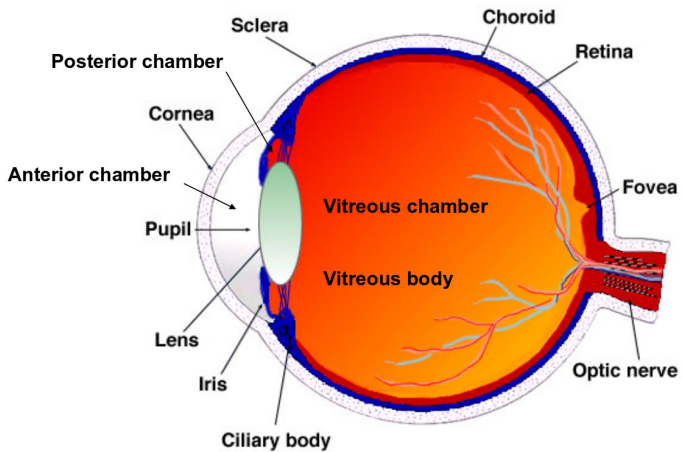
1 Introduction

2 Stability of the interface between aqueous humor and vitreous substitutes after vitreoretinal surgery

3 Flow of aqueous humour with an intraocular lens

4 References

Anatomy of the eye



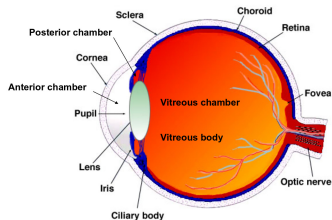
Vitreous characteristics and functions

Vitreous composition

The main constituents are

- Water (99%);
- hyaluronic acid (HA);
- collagen fibrils.

Its structure consists of long, thick, non-branching collagen fibrils suspended in hyaluronic acid.



Normal vitreous characteristics

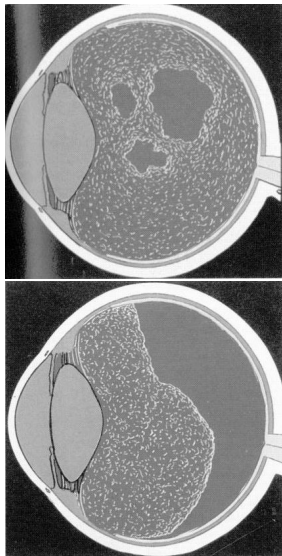
- The healthy vitreous in youth is a gel-like material with **visco-elastic mechanical properties**, which have been measured by several authors (Lee et al., 1992; Nickerson et al., 2008; Swindle et al., 2008).
- In the outermost part of the vitreous, named **vitreous cortex**, the concentration of collagen fibrils and HA is higher.
- The vitreous cortex is in contact with the **Internal Limiting Membrane (ILM)** of the retina.

Physiological roles of the vitreous

- **Support function for the retina** and filling-up function for the vitreous body cavity;
- **diffusion barrier** between the anterior and posterior segment of the eye;
- establishment of an **unhindered path of light**.

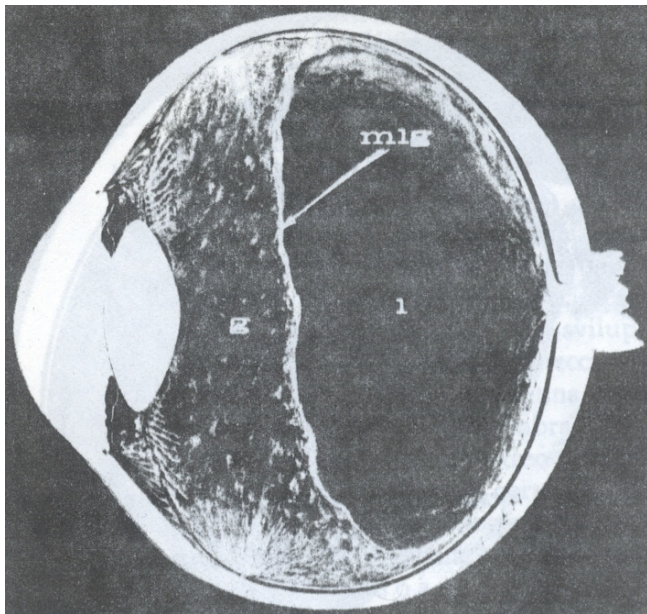
Vitreous ageing

With advancing age the vitreous typically undergoes significant changes in structure.

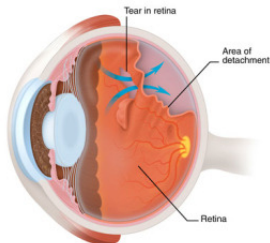


- Disintegration of the gel structure which leads to **vitreous liquefaction (synchysis)**. This leads to an approximately linear increase in the volume of liquid vitreous with time. Liquefaction can be as much extended as to interest the whole vitreous chamber.
- Shrinking of the vitreous gel (**syneresis**) leading to the detachment of the gel vitreous from the retina in certain regions of the vitreous chamber. This process typically occurs in the posterior segment of the eye and is called **posterior vitreous detachment (PVD)**. It is a pathophysiologic condition of the vitreous.

Partial vitreous liquefaction



Retinal detachment



Posterior vitreous detachment (PVD) and vitreous degeneration:

- more common in myopic eyes;
- preceded by changes in vitreous macromolecular structure and in vitreoretinal interface → possibly mechanical reasons.
- If the retina detaches from the underlying layers → loss of vision;

Rhegmatogenous retinal detachment:

- fluid enters through a retinal break into the sub retinal space and peels off the retina.

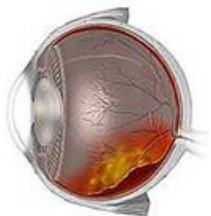
Risk factors:

- **myopia**;
- posterior vitreous detachment (PVD);
- lattice degeneration;
- ...

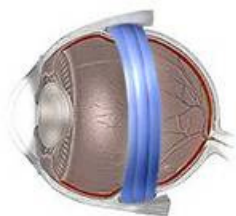
Scleral buckling and vitrectomy

Scleral buckling

Before



After



Scleral buckling is the application of a rubber band around the eyeball at the site of a retinal tear in order to promote reattachment of the retina.

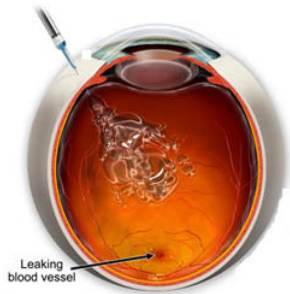
Vitrectomy



The vitreous may be completely replaced with tamponade fluids: silicon oils, water, gas, ..., usually immiscible with the eye's own aqueous humor

Intravitreal drug delivery

It is difficult to transport drugs to the retina from 'the outside' due to the tight blood-retinal barrier → use of **intravitreal drug injections**.



Diffusion is usually understood as the principal source for drug delivery, what about **advection** ?

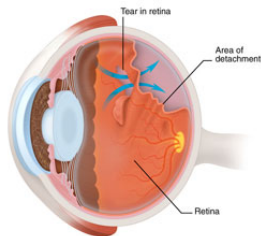
Motivations of the work

Why do research on vitreous motion?

- Possible connections between the mechanism of **retinal detachment** and
 - the shear stress on the retina;
 - flow characteristics.
- Especially in the case of liquefied vitreous eye rotations may produce effective **fluid mixing**. In this case **advection may be more important than diffusion** for mass transport within the vitreous chamber.
Understanding diffusion/dispersion processes in the vitreous chamber is important to predict the behaviour of drugs directly injected into the vitreous.

Stability of the interface between aqueous humor and vitreous substitutes after vitreoretinal surgery

Retinal detachment



Warning signs of retinal detachment:

- Flashing lights.
- Sudden appearance of floaters.
- Shadows on the periphery of your vision.
- Gray curtain across your field of vision.

Vitrectomy



The vitreous may be completely replaced with tamponade fluids: silicon oils, water, gas, ...

- Denoted **tamponade liquids**
- Purpose: Induce an instantaneous interruption of an open communication between the subretinal space/retinal pigment epithelial cells and the pre-retinal space.
- Healing: a scar should form as the cells absorb the remaining liquid.

Fluids commonly used as a vitreous substitutes

- **Silicone oils;**

- $960 \leq \rho^* \leq 1290 \text{ kg/m}^3$
- $10^{-4} \leq \nu^* \leq 5 \times 10^{-3} \text{ m}^2/\text{s}$
- $\sigma^* \approx 0.05 \text{ N/m}$

- **Perfluorocarbon liquids;**

- $1760 \leq \rho^* \leq 2030 \text{ kg/m}^3$
- $8 \times 10^{-7} \leq \nu^* \leq 8 \times 10^{-6} \text{ m}^2/\text{s}$
- $\sigma^* \approx 0.05 \text{ N/m}$

- **Semifluorinated alkane liquids;**

- $1350 \leq \rho^* \leq 1620 \text{ kg/m}^3$
- $4.6 \times 10^{-4} \leq \nu^* \leq 10^{-3} \text{ m}^2/\text{s}$
- $0.035 \leq \sigma^* \leq 0.05 \text{ N/m}$

The choice of tamponade liquid depends on the specific case

- The tabulated fluids are **immiscible** with water and commonly used in surgery
- A lighter fluid (cf. water) is used to tamponade in the upper part
- A heavier fluid is used to tamponade in the lower part
- High surface tension is preferred to a low value (**EXPERIENCE**)
- High value of viscosity (cf. water) is preferred to a low value (**EXPERIENCE**)

What could happen otherwise ?

Emulsification

Emulsification leads to loss of vision, **not satisfactory**

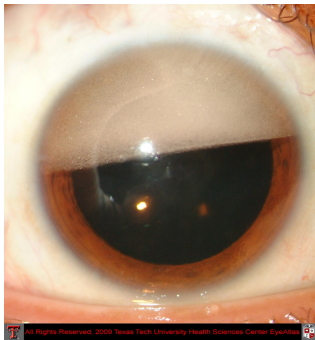


Figure: Emulsification of vitreous substitutes in the vitreous chamber

Summary & Motivation

Summary

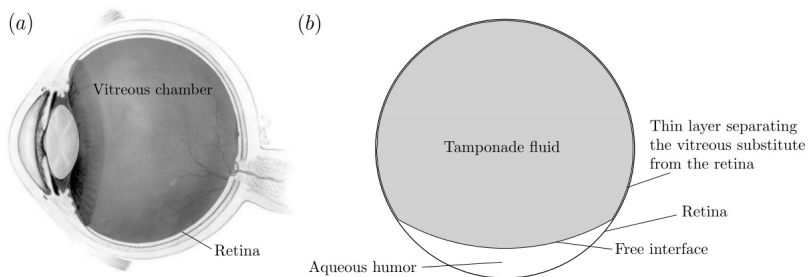
- From **experience** it is known that tamponade fluids with **high surface tension** and **high viscosity** (compared to water) are less prone to emulsify
- It is also known that initially "good" tamponade fluids tend to change with time, for instance a decrease of surface tension due to **surfactants**, which leads to emulsification.
- It is generally believed that **shear stresses** at the tamponade fluid-aqueous **interface** generated during eye rotations play a crucial role in the generation of an emulsion.
- The tamponade liquid needs to stay for a period of months so it is of interest to know how emulsification can be avoided.

Our analysis

- We want to understand how emulsification, or the initial stages leading to emulsification, are related to the parameters (surface tension, viscosity, density, real conditions).
- As a first study we focus on the **stability characteristics of the interface** in order to see if it has any role.
- A linear stability analysis, of wave like solutions, is used.
- The evolution of the disturbance kinetic energy is analyzed.

Mathematical model I

The geometry



Mathematical model II

Underlying assumptions

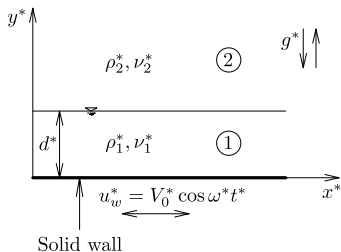


Figure: Geometry of the problem

- $d^* \ll R^*$
- 2D-model;
- flat wall oscillating harmonically;
- semi-infinite domain;
- small perturbations;
- quasi-steady approach.
- Stokes problem when $\{\}_{1} = \{\}_{2}$

Scaling and Dimensionless Parameters

$$\mathbf{x} = \frac{\mathbf{x}^*}{d^*}, \quad \mathbf{u}_i = \frac{\mathbf{u}_i^*}{V_0^*}, \quad p_i = \frac{p_i^*}{\rho_1^* V_0^{*2}}, \quad t = \frac{V_0^*}{d^*} t, \quad \omega = \frac{d^*}{V_0^*} \omega^*$$

$$m = \frac{\mu_2^*}{\mu_1^*}$$

$$\gamma = \frac{\rho_2^*}{\rho_1^*}$$

$$Re = \frac{V_0^* d^*}{\nu_1^*}$$

$$Fr = \frac{V_0^*}{\sqrt{g^* d^*}}$$

$$S = \frac{\sigma^*}{\rho_1^* d^* V_0^{*2}}$$

Basic flow

Analytical solution

Parallel time-dependent flow

$$U_1(y, t) = (c_1 e^{-ay} + c_2 e^{ey}) e^{i\omega t} + c.c.,$$

$$U_2(y, t) = c_3 e^{-by} e^{i\omega t} + c.c.,$$

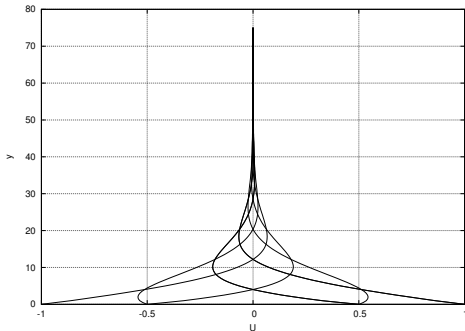
$$\frac{\partial P_1}{\partial y} = -Fr^{-2},$$

$$\frac{\partial P_2}{\partial y} = -\gamma Fr^{-2},$$

where

$$a = \sqrt{i\omega R}, \quad b = \sqrt{\frac{i\gamma\omega R}{m}}.$$

and c_1, c_2, c_3 are functions of a, b, m .



Linear stability analysis

Flow decomposition:

$$u_i = U_i + u_i', \quad v_i = v_i' \quad p_i = P_i + p_i'$$

Boundary conditions:

$$u_1'(0, t) = v_1'(0, t) = 0 \quad \text{and} \quad u_2'(y, t) \rightarrow 0, \quad v_2'(y, t) \rightarrow 0 \quad \text{as} \quad y \rightarrow \infty$$

Interface: ($y^* = d^*$) introducing also the perturbation of the interface η'

- Continuity of the perturbation velocity components across the interface
- Continuity of the tangential stress of across the interface
- The wall normal stress is balanced by the surface tension

A quasi-steady approach is assumed with two-dimensional wave-like solutions as:

$$\xi_i = e^{i\alpha(x - \Omega t)} \hat{\xi}_i(y, \tau) + c.c$$

where

$$0 \leq \tau \leq 2\pi/\omega$$

The system of equations is reduced introducing the perturbation stream function giving **two Orr-Sommerfeld equations**, discretized using finite differences, solved using an inverse iteration algorithm.

Range of variability of the dimensionless parameters

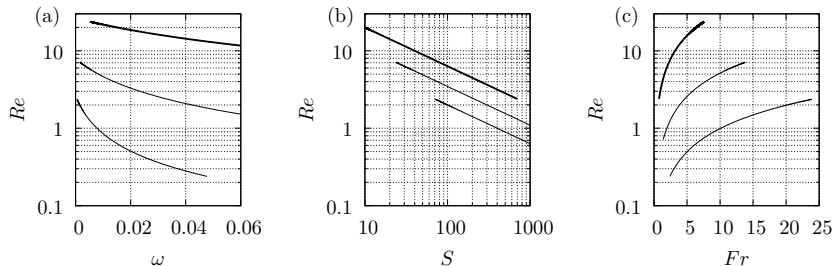


Figure: Relationship between $Re - \omega$, $Re - S$ and $Re - Fr$ obtained adopting feasible values of eye movement. From thin to thick curves: $d = 1 \times 10^{-5} \text{ m}$, $d = 3 \times 10^{-5} \text{ m}$, $d = 1 \times 10^{-4} \text{ m}$

Neutral Curves

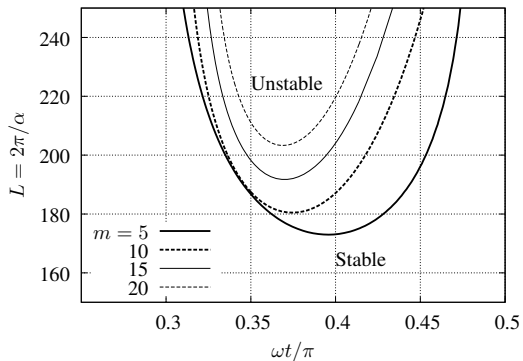


Figure: $S = 14$, $\gamma = 1.0$, $R = 7$, $\omega = 0.001$

Energy analysis

The disturbance kinetic energy is given by 3 contributions: production, dissipation and interface related terms

$$\begin{aligned}
 \frac{\alpha}{2\pi} \frac{dE}{dt} = & - \int_0^1 u_1 v_1 U_1' dy - \gamma \int_1^{+\infty} u_2 v_2 U_2' dy \\
 & - \frac{1}{Re} \int_0^1 \left[\left(\frac{\partial u_1}{\partial x} \right)^2 + \left(\frac{\partial u_1}{\partial y} \right)^2 + \left(\frac{\partial v_1}{\partial x} \right)^2 + \left(\frac{\partial v_1}{\partial y} \right)^2 \right] dy \\
 & - \frac{m}{Re} \int_1^{+\infty} \left[\left(\frac{\partial u_2}{\partial x} \right)^2 + \left(\frac{\partial u_2}{\partial y} \right)^2 + \left(\frac{\partial v_2}{\partial x} \right)^2 + \left(\frac{\partial v_2}{\partial y} \right)^2 \right] dy \\
 & \left(v_1 \left[(\gamma - 1) Fr^{-2} + \alpha^2 S \right] \eta - \frac{v_1}{Re} \left(\frac{\partial v_1}{\partial y} - m \frac{\partial v_2}{\partial y} \right) + \frac{1}{Re} \left(u_1 \frac{\partial u_1}{\partial y} - m u_2 \frac{\partial u_2}{\partial y} \right) \right) \Big|_{y=1}. \quad (4)
 \end{aligned}$$

The different contributions of (4) are commonly presented in terms of growth rates. The sum can directly be compared with the solution of the eigenvalue problem governing the linear stability problem.

$$\frac{1}{2\alpha E} \frac{dE}{dt} = \text{Im}(\Omega).$$

Results from the energy analysis

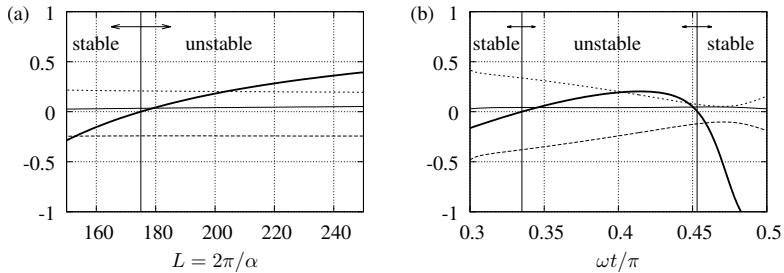


Figure: The different contributions from the energy analysis as a function of (a) L for $\omega t/\pi = 0.4$ (a) and (b) $\omega t/\pi$ for $L = 200$. In both figures $S = 14$, $\gamma = 1.0$, $R = 7$, $m = 5$, $\omega = 0.001$. Lines: thin solid (production), dashed (dissipation), dotted (interface), thick solid (growth rate scaled).

Shortest unstable wave length

The **shortest** unstable wave length as a function of S , Re and γ .

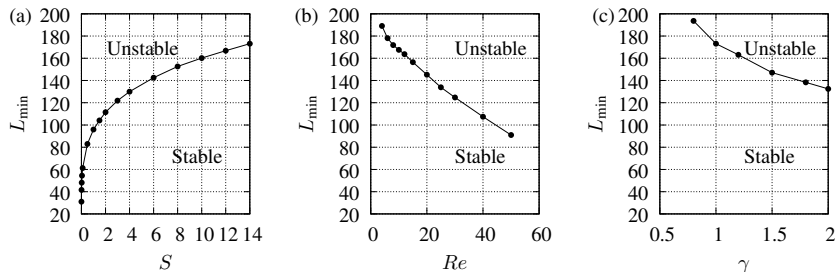


Figure: Length of the shortest unstable perturbation L_{min} versus S (a), Re (b), and γ (c) with $\omega = 0.001$ and $m = 5$. The values of $Re = 7$ in (a) and (c), $S = 14$ in (b) and (c), and $\gamma = 1$ in (a) and (b), respectively.

Verification of the quasi-steady approach

In order for the quasi steady approach to be valid the perturbation frequency should be larger than the base flow frequency (scale separation).

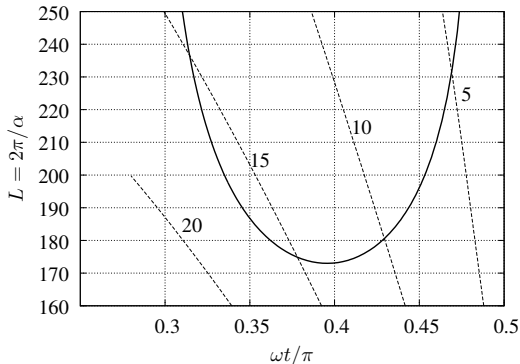


Figure: Neutral stability curve (solid line) in the $(\omega t/\pi) - L$ plane for the case $m = 5$, $Re = 7$, $\omega = 0.001$, $S = 14$, $\gamma = 1$. The dotted lines show the values of the ratio $\alpha \Re(\Omega)/\omega$.

Conclusions and Continuation

Monitoring the shortest unstable wave length (critical wave length) we have seen that:

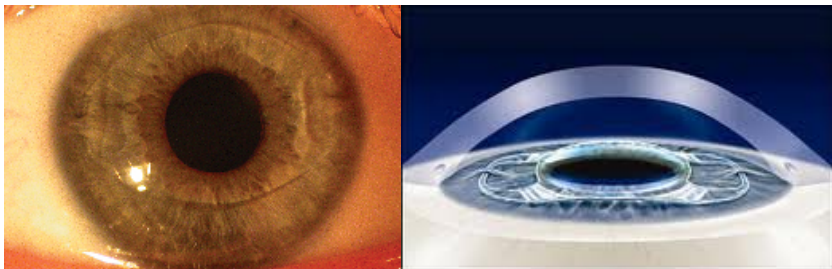
- Increasing the viscosity, ratio the critical wave length increases (**stabilizing for the Eye**)
- Increasing the surface tension, the critical wave length increases (**stabilizing for the Eye**)
- Increasing the Reynolds no., the critical wave length decreases (**destabilizing for the Eye**)
- Increasing the density ratio, the critical wave length decreases (**destabilizing for the Eye**)
- The first two is "in line" with realistic observations.
- For realistic values of $R, S, \gamma, m, \omega, d^*$ the critical wave length ≈ 5 mm, which is about half the Eye radius.
- However, the growth rate is instantaneous and the waves unstable only during certain intervals of one period. (cf. turbulent burst in the classical Stokes II problem). No sustained growth over one period is guaranteed.
- This analysis is far from explaining the onset of emulsion but a first step to rule out (or not) different physical mechanisms.

Next step...

- Floquet analysis
- Non-modal analysis
- Include curvature,, more realistic geometry (circle, sphere)

Flow of aqueous humour with an intraocular lens

Phakic intraocular lenses



Motivation

Intraocular lenses decrease endothelial cell density in some patients. Possible reasons include:

- Excess shear stress due to altered flow of aqueous
- Impaired transport of nutrients due to altered flow
- Non-ideal placement of lens, with respect to iris and other tissues
- Impact of external body on eye (e.g. accidental impact, patient touching eyes)

This study: Investigate the first possibility, by comparing the shear stress both in the presence of and without the lens. Moreover, monitor the intra-ocular pressure (IOP).

Description of the model

Governing equations:

$$\nabla \cdot \mathbf{u} = 0$$

$$\rho \left(\frac{\partial \mathbf{u}}{\partial t} + \mathbf{u} \cdot \nabla \mathbf{u} \right) = -\nabla p + \nabla^2 \mathbf{u} + \rho \mathbf{g}$$

$$\rho c_p \left(\frac{\partial T}{\partial t} + \mathbf{u} \cdot \nabla T \right) = k_a \nabla^2 T$$

Assumptions:

- Boussinesq approximation (ρ is constant, except in the gravitational acceleration term in which $\rho = \rho_0(1 - \alpha(T - T_0))$)

Numerical solution:

- All solutions are obtained with *OpenFOAM*
- Solvers were first tested on cases where analytical solutions exist.

Definitions:

Symbol	Definition
\mathbf{u}	velocity
p	pressure
ρ	density of aqueous
μ	viscosity of aqueous
\mathbf{g}	acceleration due to gravity
c_p	specific heat at constant pressure
T	temperature
k_a	thermal conductivity of aqueous

Model geometry

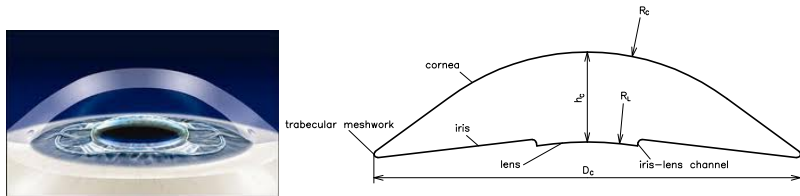


Figure: (left) "real" anterior chamber, (right) cross-section of the idealized anterior chamber used in the simulations.

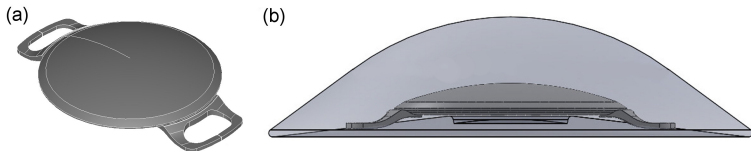


Figure: (a) Geometry of the pIOL consisting of a lens and two haptics that have claws that allow the lens to be attached to the iris, (b) pIOL placed in the anterior chamber.

Flow mechanisms

Flow induced by aqueous production/drainage:

Aqueous humor is produced by the ciliary body, and then flows through the posterior chamber, the pupil and the anterior chamber, from where it is drained into the trabecular meshwork. ($3 \mu\text{l}/\text{min}$)

Flow induced during miosis:

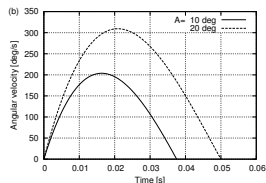
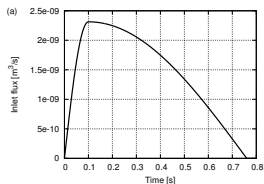
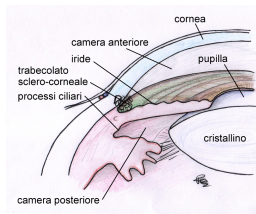
During pupil contraction (miosis), a flow from the posterior to the anterior chamber of the eye is generated, which is intense, although it only lasts a short time, typically less than 1 s. (middle figure)

Buoyancy-driven flow:

It is well known that, since the posterior surface of the cornea is typically cooler than the iris and lens. We prescribed a temperature of 34°C on the cornea and 37°C on all other surfaces.

Flow induced by saccades of the eye:

We consider the flow generated in the anterior chamber by rotations of the eye bulb by modeling isolated rotations using the analytical relationship proposed by Repetto et al. (2005) which provides the angular velocity of the eye as a function of time. (bottom figure)



Flow induced by aqueous production and drainage

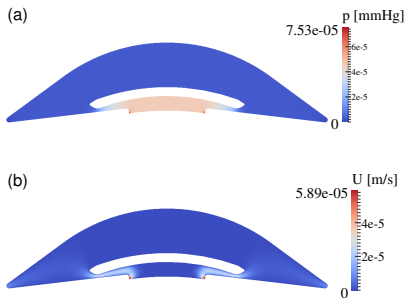


Figure: Flow due to production/drainage of aqueous humor with the device present: (a) excess pressure above IOP, (b) velocity magnitude.

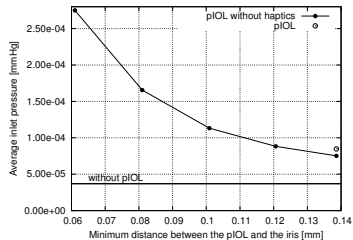


Figure: Average pressure drop between iris–lens channel and trabecular meshwork as a function of the minimum distance between the pIOL and the iris (solid circles). No pIOL (horizontal line) and pIOL with haptics (empty circle).

Lubrication theory:

$$\Delta p = \frac{6\mu Q}{\pi} \int_{r_1}^{r_2} \frac{dr}{rh^3},$$

To get $\Delta p = 1 \text{ mmHg}$ you need $h = 1 \mu\text{m}$

Flow induced during miosis

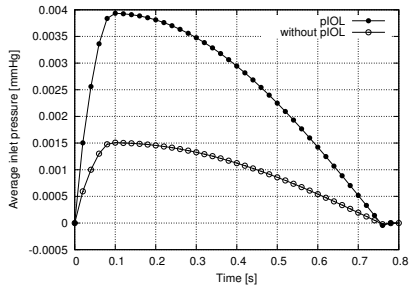


Figure: Spatially averaged pressure over the inlet as a function of time during miosis, in an eye both with the pIOL (solid circles) and without it (open circles).

Buoyancy-driven flow I

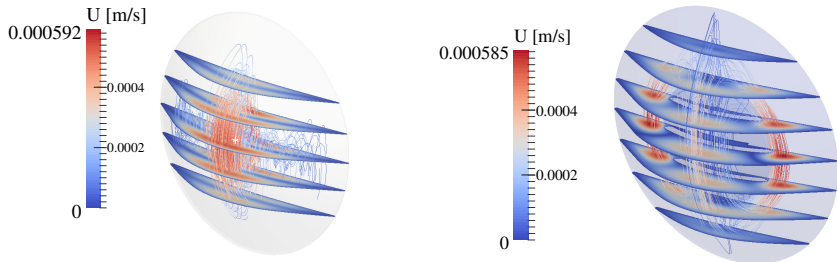


Figure: Buoyancy-driven flow in the absence of the pIOL. Gravity acts in the vertical direction. Streamlines of the flow and the distribution of the velocity magnitude on selected horizontal planes, (a) without the lens, (b) with the lens.

Buoyancy-driven flow II

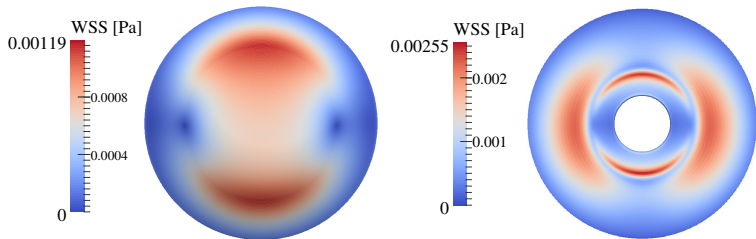


Figure: Buoyancy-driven flow in the presence of the pIOL. (a) Magnitude of WSS on the cornea; (b) WSS on the iris.

Buoyancy-driven flow III

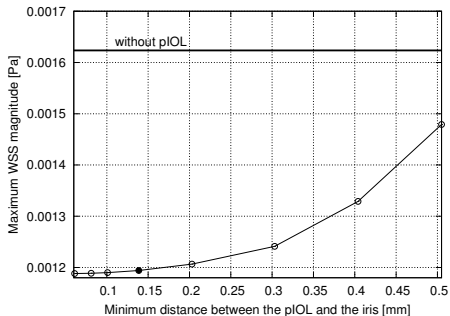


Figure: Spatial maximum of the WSS on the cornea as a function of the distance between the pIOL and the iris, neglecting the haptics (open circles). The maximum WSS with no pIOL is shown by the horizontal line, whilst the maximum WSS with the pIOL in its normal position and including the haptics is shown by the solid circle.

Flow induced by saccades of the eye

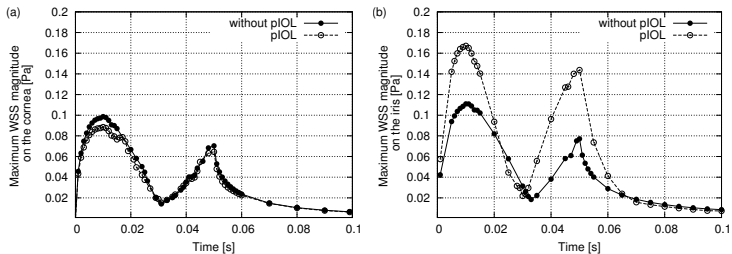


Figure: Time evolution of the spatial maximum of the WSS on the (a) cornea and (b) iris in an eye performing a saccade of angle 10° .

Discussion and conclusions

- (i) If the lens is properly placed there is a negligible influence on the pressure in the posterior chamber.
- (ii) There is no significant increase of the WSS on the cornea.
- (iii) The WSS on the iris is significantly greater than in the case with no pIOL, but the increase is not likely to be sufficiently great so as to give a risk of cell detachment.

Endothelial cell loss:

- Kaji et al.(2005) performed experiments on porcine corneal endothelial cells that were plated onto glass slides, and found that significant detachment was observed for shear stresses in excess of 0.03 Pa if the cells had had 1 hour of adhesion, rising to 0.1 Pa for 3 hours of adhesion. Our model predicts that the actual values are significantly smaller than this.
- Other causes: **rubbing** the eye (mechanical forcing), insufficient delivery of oxygen **and/or nutrients** to the corneal epithelium. The latter will be studied in the near future.

References I

- B. Lee, M. Litt, and G. Buchsbaum. Rheology of the vitreous body. Part I: viscoelasticity of human vitreous. *Biorheology*, 29:521–533, 1992.
- C. S. Nickerson, J. Park, J. A. Kornfield, and H. Karageozian. Rheological properties of the vitreous and the role of hyaluronic acid. *Journal of Biomechanics*, 41(9):1840–6, 2008. doi: 10.1016/j.jbiomech.2008.04.015.
- K. Swindle, P. Hamilton, and N. Ravi. In situ formation of hydrogels as vitreous substitutes: Viscoelastic comparison to porcine vitreous. *Journal of Biomedical Materials Research - Part A*, 87A(3):656–665, Dec. 2008. ISSN 1549-3296.